Environmental Pollution 182 (2013) 343–356

Contents lists available at ScienceDirect

Environmental Pollution

journal homepage: www.elsevier.com/locate/envpol

Ozone distribution in remote ecologically vulnerable terrain of the southern Sierra Nevada, CA

Jeanne Panek [a,*,1], David Saah [b], Annie Esperanza [c], Andrzej Bytnerowicz [d], Witold Fraczek [e], Ricardo Cisneros [f]

[a] Center for Forestry, University of California, Berkeley, CA 94720, USA
[b] Spatial Informatics Group, 3248 Northampton Ct., Pleasanton, CA 94588, USA
[c] Sequoia and Kings Canyon National Parks, 47050 Generals Highway, Three Rivers, CA 93271, USA
[d] USDA-Forest Service, Pacific Southwest Research Station, 4955 Canyon Crest Drive, Riverside, CA 92507, USA
[e] ESRI, 380 New York St., Redlands, CA 92373, USA
[f] USDA-Forest Service, Sierra National Forest, 1600 Tollhouse Rd., Clovis, CA 93611, USA

ARTICLE INFO

Article history:
Received 27 March 2013
Received in revised form
18 July 2013
Accepted 20 July 2013

Keywords:
Ozone
Landscape-scale spatial analysis
Forests
Vulnerability
Passive samplers

ABSTRACT

Ozone concentration spatial patterns remain largely uncharacterized across the extensive wilderness areas of the Sierra Nevada, CA, despite being downwind of major pollution sources. These natural areas, including four national parks and four national forests, contain forest species that are susceptible to ozone injury. Forests stressed by ozone are also more vulnerable to other agents of mortality, including insects, pathogens, climate change, and ultimately fire. Here we analyze three years of passive ozone monitor data from the southern Sierra Nevada and interpolate landscape-scale spatial and temporal patterns during the summer-through-fall high ozone concentration period. Segmentation analysis revealed three types of ozone exposure sub-regions: high, low, and variable. Consistently high ozone exposure regions are expected to be most vulnerable to forest mortality. One high exposure sub-region has been documented elsewhere as being further vulnerable to increased drought and fire potential. Identifying such hot-spots of forest vulnerability has utility for prioritizing management.

1. Introduction

The poor air quality in many parts of the southern Sierra Nevada mountain range in California is a result of major upwind pollution sources. While the ozone concentrations of the adjacent populated landscape are well-characterized and continuously monitored (CARB, 2013), the ozone concentrations of the extensive downwind wilderness areas in the Sierra Nevada remain largely unmapped. These natural areas, including four national parks and four national forests (Supplementary Data Fig. 1), contain ecosystem types that have been documented as being vulnerable to ozone pollution (Miller and Millecan, 1971; Duriscoe, 1990; Arbaugh et al., 1998; Bytnerowicz et al., 2003a,b). While significant direct injury to these forests from ozone pollution has been reported, forests that have been stressed by ozone are also more vulnerable to other agents of mortality, including insects (Stark et al., 1968; Eatough Jones et al., 2004), pathogens (James et al., 1980; Fenn et al., 1990), climate (Weaver et al., 2009) and ultimately fire (Van Mantgem et al., 2003; Grulke et al., 2009).

The goal of this study was to develop a map of ozone exposure across wilderness areas in the heavily ozone-impacted southern Sierra Nevada, with an eye toward identifying ecosystems that are left vulnerable to other agents of mortality by ozone exposure.

The foothill and mountain ecosystems of the Sierra Nevada lie along the eastern edge of the San Joaquin Valley Air Basin (Fig. 1), the southern half of California's broad central valley, which is classified as "extreme non-attainment", the worst category relative to federal standards of ozone (USEPA, 2011). The San Joaquin Valley accounts for about 14 percent of total California statewide emissions (CARB, 2010). Generalized surface airflow patterns carry pollutants southeastward from their sources into major drainages in the Sierra Nevada, as well as in a large counterclockwise eddy northward along their western flank (Fig. 1).

Combining data from real-time, continuous ozone monitoring networks with GIS-based spatial interpolation models has

* Corresponding author.
E-mail address: jeanne.panek@gmail.com (J. Panek).
[1] Present address: Panek and Associates Ecological Consulting, 2311 Webster St., Berkeley, CA 94705, USA.

0269-7491/$ – see front matter © 2013 Elsevier Ltd. All rights reserved.
http://dx.doi.org/10.1016/j.envpol.2013.07.028

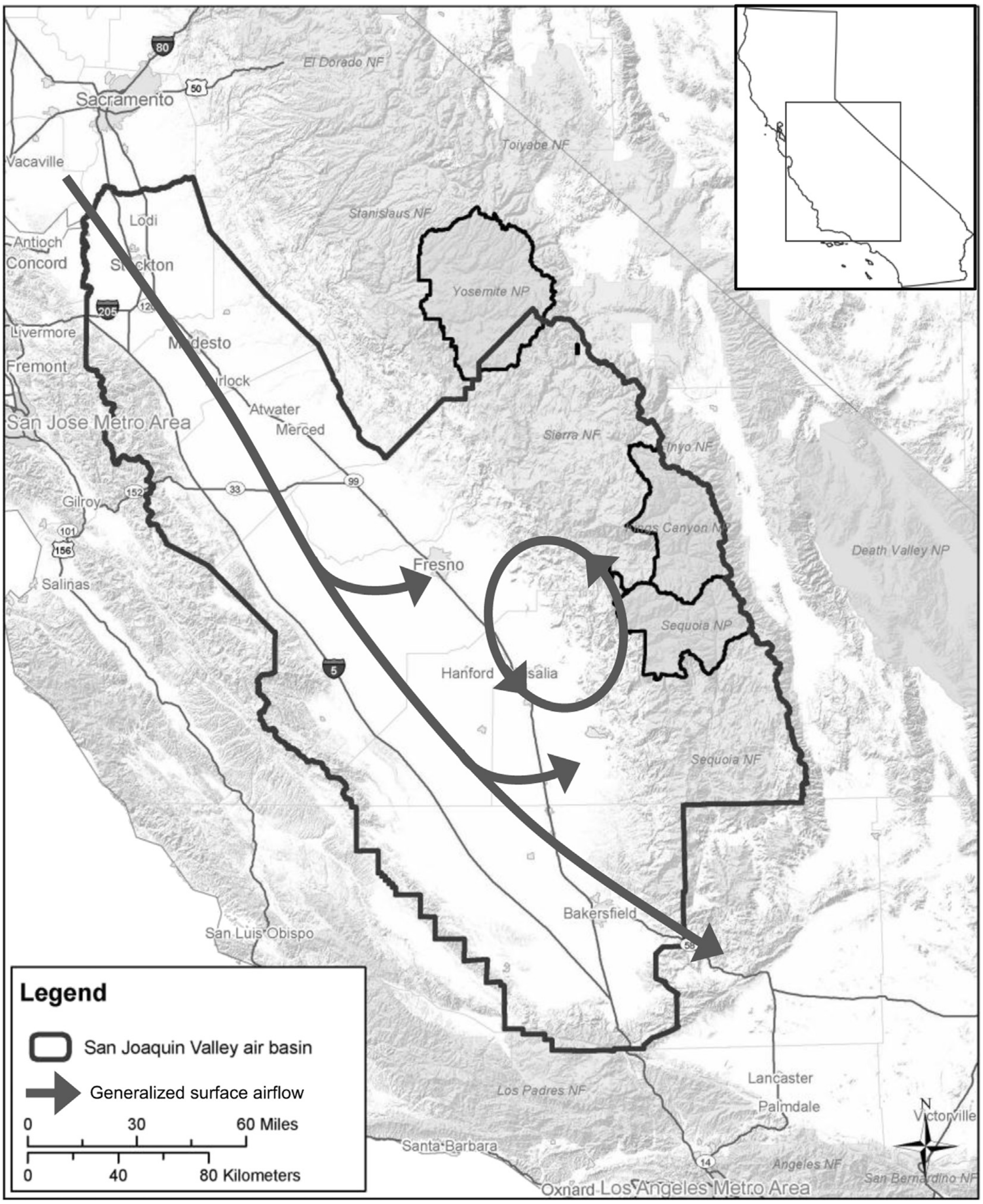

Fig. 1. The San Joaquin Valley air basin. Arrows show general surface airflow patterns, including an eddy that circulates counterclockwise along the western front of the Sierra Nevada.

established a powerful approach to estimating ozone concentration surfaces over broad, populated landscapes in Europe and the U.S. (Loibl et al., 1994; Wong et al., 2004; De Marco et al., 2010; Denby et al., 2011; Singh et al., 2011). Estimating landscape-scale ozone concentrations in remote mountainous terrain is difficult, however, due to steep elevational gradients, heterogeneous terrain, complex wind and deposition patterns, and the lack of power/access needed to maintain continuous monitors. Passive sampler networks can provide coarse seasonal and spatial ozone concentration dynamics across these large areas. These networks integrate ozone concentrations over long periods and can be a critical element of characterizing ozone concentration in complex terrain (Krupa and Legge, 2000). Following the approach used with continuous monitor networks, we sought to combine data from a passive monitor network with a spatial interpolation model that included parameters suitable for the southern Sierra Nevada, to estimate ozone surfaces over this remote, ecologically-vulnerable landscape. Parameters influencing ozone concentrations can vary spatially, daily and seasonally. Uptake by, and impacts on, vegetation are further complicated by daily and seasonal plant physiological patterns that influence ozone uptake (Panek, 2004; Panek and Goldstein, 2001).

1.1. Climate drivers of ozone concentration

The Mediterranean climate of California influences timing and distribution of ozone. In the Sierra Nevada, precipitation falls mainly between October and June. The summer months are generally dry and hot. High summertime temperatures and greater solar radiation lead to higher ozone concentrations in the summer months (Van Ooy and Carroll, 1995; Bytnerowicz et al., 2002). Isolated rainstorms may temporarily scrub ozone from the air. A combination of rising temperatures, solar radiation and water availability in spring and early summer months enhances Sierra Nevada forest physiological activity (Panek, 2004), which has the potential to remove ozone from the air and thus decrease atmospheric concentrations. Surface wind patterns move ozone and its precursors through the San Joaquin Valley Air Basin and force it upslope in the Sierra Nevada. These patterns are influenced by temperature and topography (Beaver et al., 2010).

1.2. Spatial drivers of ozone concentration

Spatial distribution of ozone across the Sierra Nevada depends on source strength, transport characteristics, topography, and surface and chemical characteristics influencing deposition (Van Ooy and Carroll, 1995; Carroll and Dixon, 2002). However, generally, ozone concentrations in the Sierra Nevada have been reported to be highest closest to the San Joaquin Valley and decrease with distance eastward and northward across the range (Preisler and Schilling, 2003; Frączek, 2003).

1.3. Fire effects on ozone concentration

Fire affects the source strength of precursors that can ultimately influence downwind ozone concentrations (Pfister et al., 2008; Bytnerowicz et al., 2013). In 2007, northern California fires in September affected ozone concentrations in northern and central parts of California and Nevada (Pfister et al., 2008). In 2008, the largest California wildfire season to date, wildfires started in late June and lasted through most of the summer season. Effects on ozone concentrations were noted in Devil's Postpile National Monument (Bytnerowicz et al., 2013). The summer of 2006 experienced a smaller wildfire season, mostly in northern California (InciWeb, 2006), and effects on ozone concentrations were undetermined.

2. Materials and methods

2.1. Passive samplers and network

Passive ozone samplers were deployed continuously over sequential two-week periods in 2006, 2007 and 2008 during the highest ozone concentrations period of the year – June through October – to estimate average 24-h ozone concentrations for each two-week period. The networks were the same in 2006 and 2007, with 38 samplers (Fig. 2, circles). In 2008, a smaller network of 18 samplers that included samplers in the eastern Sierra Nevada was deployed (Fig. 2, triangles). Samplers were distributed over a broad area of the southern Sierra Nevada including multiple natural resource management jurisdictions (Supplementary Fig. 1). A description of Ogawa passive ozone samplers, and methods for calculating the 24-h average ozone concentration, can be found in Koutrakis and Kelly (1993).

2.2. Defining the analysis region

The extent of the ozone analysis boundary was determined by a scientifically supported, standardized definition for "ecological region" which was developed as part of an ongoing natural resource analysis collaboration between federal management agencies, universities, and non-governmental organizations in the southern Sierra Nevada (NPS 2013). The region was defined in a series of steps described in detail in Thorne et al. (2013) as a spatial overlay of the major biotic and abiotic landscape features that are integral to understanding the relationship between a protected area and its surrounding ecosystems, including watersheds, natural disturbances, and crucial and contiguous habitat for select species.

2.3. Geospatial regression

Geographically weighted regression (GWR) is one of several spatial regression techniques. GWR provides a local model of a variable or process by fitting a regression equation to every feature in the dataset. In this study both ordinary least squares (OLS) regression and GWR approaches were tested to build an ozone regression from a selection of independent variables.

The GWR models provided a better fit than the OLS models and were used for the analysis. Regression kriging was also considered, but ultimately determined inappropriate. Like geographically weighted regression (GWR), regression kriging (RK) is a powerful local spatial prediction model (Singh et al., 2011; Denby et al., 2011), however the samples used in this analysis were not spatially uniform and were non-stationary, thus GWR provided a more flexible estimation of parameters. Geographically weighted regression emphasizes spatial non-stationarity, but takes no account of spatial correlation. An adaptive kernel sampling was used to calculate the weight. The RK approach would use the weight matrix and the spatial semivariogram for regression parameter estimation, determined by an optimal semivariogram function that quantitatively models the spatial dependence and structure. The RK approach would have been problematic with the sampling design and model variables used.

All the GWR analyses were run using an adaptive kernel that searched for an optimal number of neighbors, selected over the fixed distance kernel based on model design constraints, and an Akaike information criterion bandwidth method. The independent variables considered for the full model included mean temperature, elevation, distance to the bottom of the nearest drainage, and maximum normalized wind velocity. Temperature and elevation were highly correlated, so only elevation was kept because of its continuous spatial coverage. The normalized wind field calculations were derived from a USDA Forest Service Joint Fire Science Program model that simulates terrain effects on wind flow at scales relevant to wildland fires and, in this case, ozone concentration (Forthofer and Butler, 2013). There is no temporal component to this variable. It is an estimate of available wind given a constant gust modified by topography and vegetation.

The same full model was applied independently to each two-week time period, with a resulting full or reduced model depending on fit. The median adjusted R^2 was 45% for all two-week periods, and the highest frequency of R^2 was in the 50–70% range.

Using the resulting geographically-weighted regression equation for that period, a continuous ozone concentration layer was extrapolated to the region, at 3500 m resolution, which is the finest resolution at which error was minimized. A separate ozone layer was made for each of the 27 two-week periods. Because ozone concentration and distribution are source- and weather-dependent, the magnitude of ozone concentration between time-periods was very different, however the distribution of ozone through each period was generally similar. The spatial average of the 27 ozone concentration layers is shown in Fig. 2.

2.4. Analysis uncertainty

Variation and uncertainty were quantified in several ways. To determine the goodness of fit of the GWR model, residuals representing the observed minus the predicted ozone concentration value at each monitoring site were analyzed for each two-week period. The absolute value of the residual at each site was normalized by the observed ozone concentration at the site and time period to allow for temporal and spatial comparison of residuals despite changes in ozone concentration over time. The annual mean and standard error of normalized residuals were calculated by site for each of the years 2006, 2007, and 2008, to show average and spread in goodness of fit. To show the variation due to ozone concentration changes over time, the standard deviation of the annual mean of modeled ozone layers was calculated within each grid cell over all measurement periods within a year.

2.5. Segmentation analysis

An Object Based Image Analysis (OBIA) segmentation algorithm was used to create 16 unique regions using eCognition® version 8.7. OBIA techniques use elements of image interpretation to automate manual interpretation of spatial data, extracting features using spectral, geometric, and contextual information in an image (Olson, 1960). Several studies have demonstrated that OBIA techniques are superior to traditional pixel-based approaches for impervious surface mapping (Thomas et al., 2003; Finke et al., 2009; Miller et al., 2009), and some have even concluded that the accuracy can approach that of manual interpretation (Kampouraki et al., 2008).

OBIA techniques focus on the application of image segmentation algorithms that group pixels into objects (Baatz and Schape, 2000). Like pixels, image objects have spectral properties (mean band values), but unlike pixels they have spatial characteristics (shape, size, texture) and are topologically aware (i.e., each object "knows" its neighbor objects). The segmentation took into consideration the variability of the input surface but not the uncertainty associated with the surface.

Regions across the landscape with high, low and variable ozone concentration classes were identified with OBIA. This analysis consisted of three major steps. The first step was to quantify the normalized variability in ozone concentrations within each raster cell. This was accomplished by quantifying a regional ozone mean then re-classifying each of the 27 two-week ozone surfaces into an above-mean or below-mean cell value. The second step then investigated the variability in ozone concentrations of step one for each cell and categorized a single surface into a high, variable, and low class. Specifically, if a cell was categorized as high 80% of the time

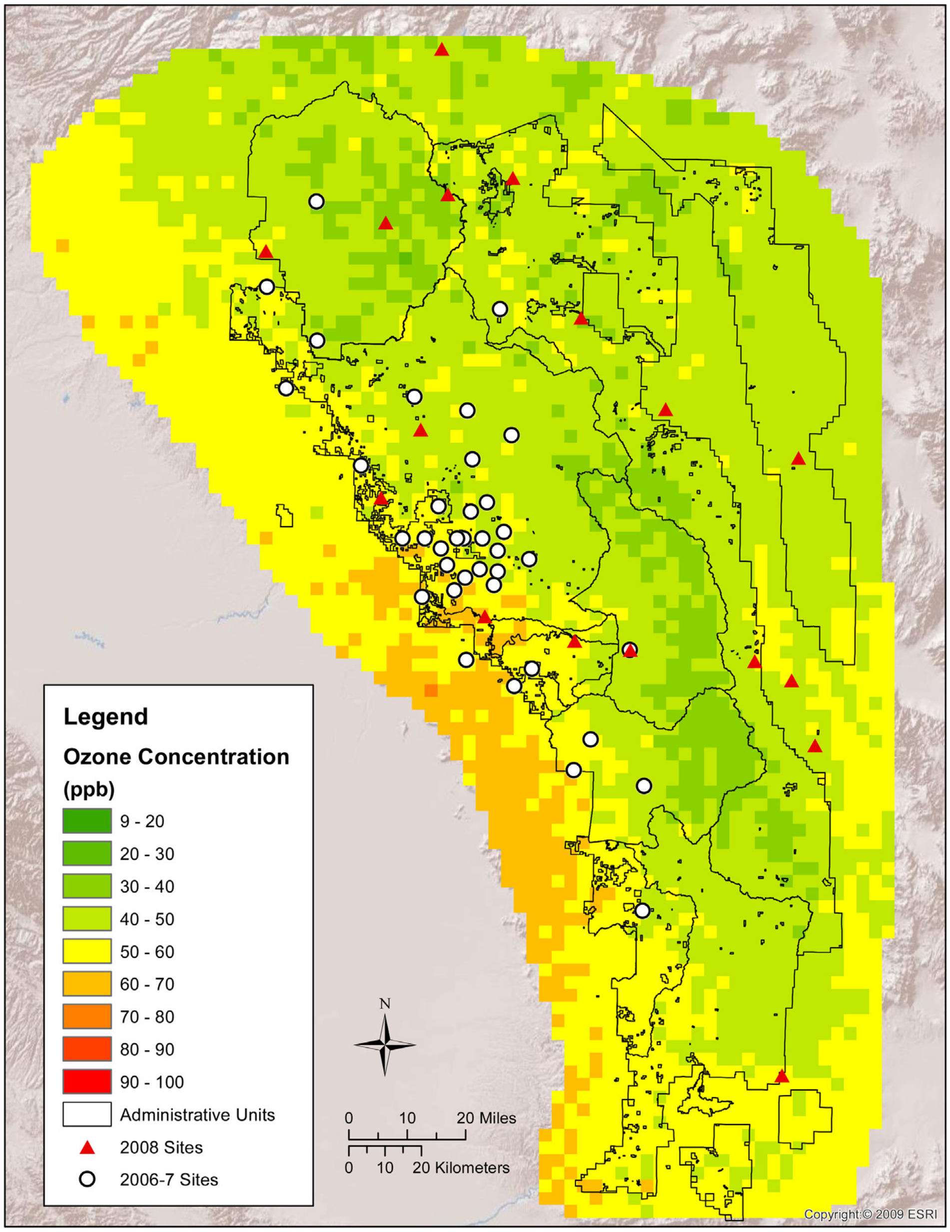

Fig. 2. Average 24-h ozone concentrations for the region, from a geographically weighted regression analysis of passive ozone monitors sampled in two-week periods over the summer and early fall months (June–October) in 2006, 2007 and 2008. Grid size is 3500 m. National forest and national park boundaries are outlined within the region. Passive ozone monitor sites are shown with circles for the 2006–7 monitoring season, and triangles for the 2008 monitoring season.

(80% of the 27 two-week ozone surfaces), it was assigned to the high classification, if it was low 80% of the time it was assigned to the low classification; otherwise it was assigned to the variable classification. Using the data from step 2 the region was then segmented into unique sub-regions of roughly 10,000 acres (40 km^2) or less, using OBIA to identify areas of similar ozone exposure.

3. Results

3.1. General spatial patterns

Average June–October ozone concentrations were generally highest on the western side of the Sierra Nevada, and highest specifically to the west of Sequoia and Kings Canyon Parks (Fig. 2), showing the influence of the sources in the San Joaquin Valley and surface airflow patterns moving southeastward toward the Sierra Nevada, as well as the recirculation effect of the counterclockwise eddy. The northern portion of the region, including Yosemite National Park, was less ozone-impacted, protected from San Joaquin Valley air basin ozone sources by distance and topography. The higher elevations of the Sierra Nevada also had low average ozone concentrations. These areas that are difficult to access, therefore have fewer sampling points, thus extrapolation to these areas was less certain. However, the pattern was consistent with the observation that the higher-elevation ozone monitoring sites in the southern Sierra Nevada generally exhibit lower ozone concentrations (Bytnerowicz et al., 2002; Panek et al., 2013). The eastern slope of the Sierra Nevada experienced incursions of ozone from the Owens Valley, so ozone concentrations were moderate there. Airflow patterns generally bring ozone to the Owens Valley through the San Joaquin River drainage to the north (Cisneros et al., 2010), and also from the Mojave Desert to the south, but concentrations were much lower than on the central western slopes.

3.2. General temporal patterns

Comparing time trends for the three years 2006–2008 using the passive sampler data revealed differences in mean ozone concentrations between years and over time (Fig. 3). Note that the 2008 monitoring network was smaller, shorter-term, and had a higher presence of Owens Valley and eastern Sierra Nevada sites.

Late summer ozone was higher in 2006 than in 2007 and 2008. All three years showed a drop in ozone mid-summer. Temperature, measured at meteorological stations near the passive sampler sites, explained 40% of the variation in measured ozone concentration over time. Rain may explain low values in years 2006 and 2008, when regional July rain events may have scrubbed ozone from the air. The drop in ozone concentration mid-summer may also be due to dynamics in source strength. Upwind fire emissions may play a role in the 2006 late July rise in ozone concentrations and the 2007 September rise. However, the largest fire season in California record to date, starting late June 2008, did not appear to greatly influence measured ozone concentrations.

3.3. Detailed spatial patterns

Looking at detailed landscape patterns of ozone concentration for each two week period allowed a closer look at regional similarities and differences over time. Figs. 4 and 5 show how concentration distribution varied over the 2006 and 2007 ozone seasons, the seasons that have the longest record.

Generally, the maps show that ozone lapped onto the lower western slopes of the Sierra Nevada much like ocean waves lapping onto a beach. Each two-week ozone period impacted the "shoreline", or the front of the range, depending on the overall magnitude of the period (Figs. 4 and 5). Generally the lower elevation western slopes of the southern Sierra Nevada received the highest ozone concentrations. However, if the period had generally higher overall ozone concentration, the "wave front" was generally greater in magnitude, the northern extent of the front had higher concentrations and the ozone wave lapped higher in elevation. However there was an area beyond the reach of the waves, the nominal "high-tide line". This break delineated a higher-elevation region that has consistently low ozone concentration from one period to the next.

Ozone penetrated into deeper river basins of the Sierra Nevada that drain west, particularly the San Joaquin River drainage, the Middle Fork of the Kings River, and the South Fork of the Kaweah River (Figs. 4 and 5). The Merced and Tuolumne Rivers, however, were an exception. Much of Yosemite and the northern interior of the study region appeared to be buffered from the brunt of ozone exposure by the topography of the extended foothill region between Yosemite National Park and the San Joaquin Valley.

A particularly interesting spatial feature was the degree of ozone penetration into the Owens Valley on the eastern side of the Sierra Nevada (Figs. 4 and 5). A wide, indefinite corridor of ozone was apparent through the San Joaquin river drainage north of Kings Canyon National Park that connects the San Joaquin Valley to the Owens Valley. Another corridor of ozone was seen from the south into the Owens Valley on the eastern side of the Sierra. Both appeared to contribute to ozone levels on the eastern side of the Sierra.

A strong feature of the spatial/temporal analysis was the general consistency of ozone distribution from one measurement period to the next. This suggested that segmentation analysis might be useful in delineating different classes of ozone exposure across the landscape.

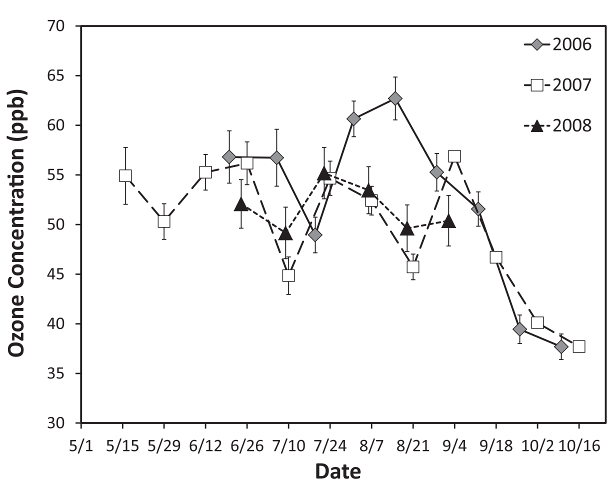

Fig. 3. Ozone concentration trends over time show differences between years, and differences in pattern over time. Ozone concentration (ppb) is shown for three years – 2006 through 2008. Dates are the beginning of two-week sample periods. Bars show standard error of the mean.

3.4. Segmentation analysis

Object-based image segmentation of all ozone events from 2006 through 2008 revealed 16 different sub-regions that fell into three categories of ozone concentration, high, variable and low (Fig. 6). The high ozone sub-regions were along the western edge of the Sierra Nevada, but including the southern portion of the range as well. The variable ozone sub-regions included the upper elevations of the western side of the Sierra Nevada as well as the Owens Valley area and other contiguous valleys on the eastern side of the mountains. The low ozone sub-regions included the higher elevations of the Sierra as well as most of Yosemite National Park.

Although each sub-region was classified as "high", "variable" and "low", some sub-regions had a greater or lesser percentage of their pixels in a given category. Sub-region 12, for example, clearly had the greatest ozone exposure of the entire region (Fig. 6). Ninety-nine percent of the pixels in sub-region 12 were in the "high" category, only 1% in the "variable" category, and none in the "low" category (Table 1). Sub-region 2, also classified as "high", had lower ozone exposure, with 73% of pixels in the "high" category and 26% in the "variable" category. Sub-region 12 is the *hottest hot-spot*. Analogously, sub-region 10 is the area with the lowest ozone exposure, i.e. the *coolest hot-spot*.

3.5. Detailed temporal patterns

The time trends of mean ozone concentration, taken from the passive sampler data and assigned to their respective geographic sub-region classifications, tracked one another over time and consistently rise and drop together (Fig. 7). This suggests that by knowing the ozone concentration over time in one sub-region class, the concentrations in other sub-regions can be generally estimated. "High" and "low" classes tracked each other most consistently, while the "variable" class, not surprisingly, tracked the least consistently, generally somewhere between the other two.

The average difference between the low and the high ozone class was 14.2 (±3.8 standard deviations) parts per billion (ppb). The average difference between the variable and the high class was 5.7 (±14.2 standard deviations) ppb. Not surprisingly, the variability in the difference between the higher and variable class was much greater.

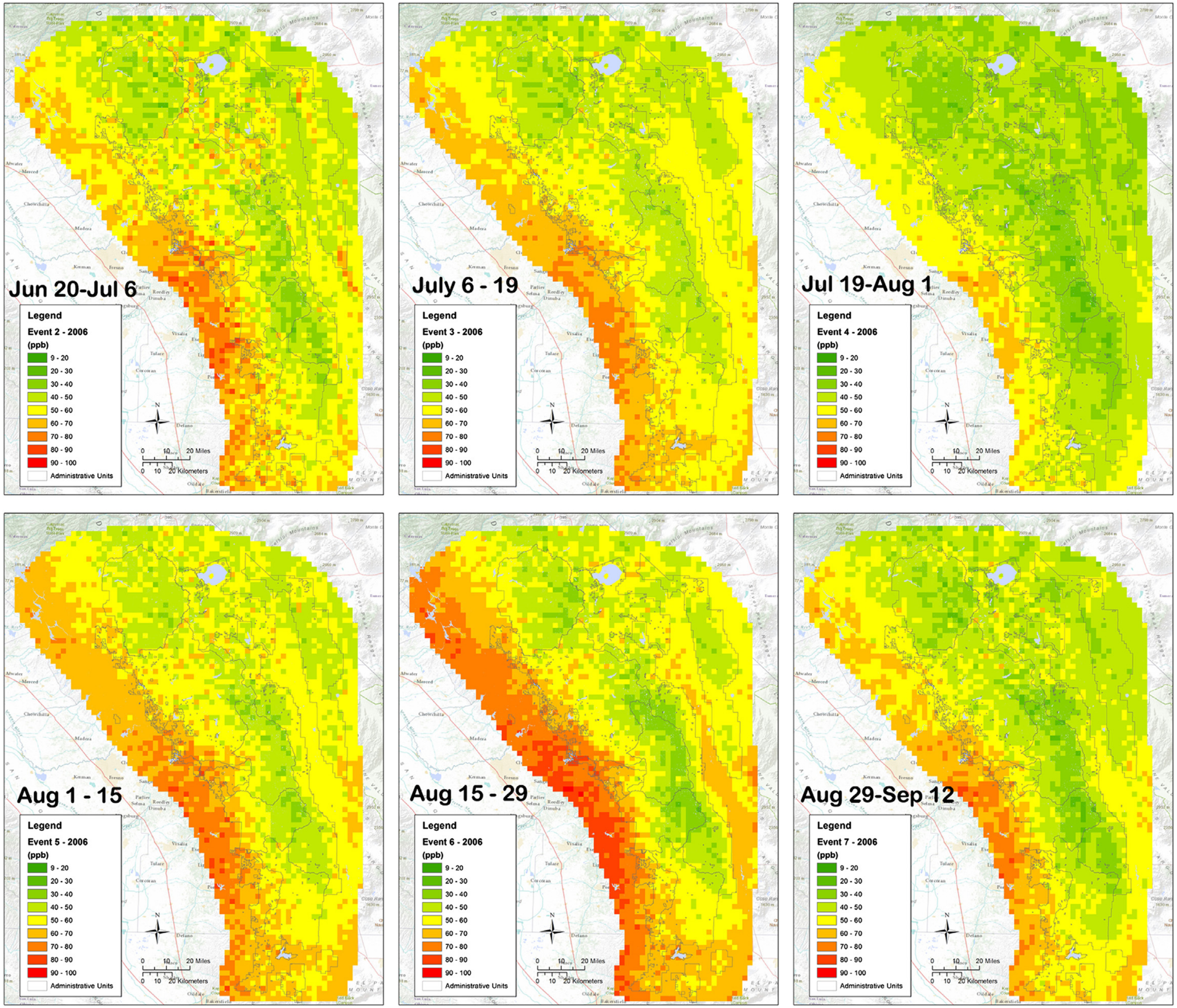

Fig. 4. Landscape patterns in ozone concentration in 2006 show temporal and spatial variation. Mean 24-h ozone concentration (ppb) for sequential two-week periods in summer-fall 2006, derived from a network of passive ozone samplers and geographically-weighted regression, are mapped across a 49,000 km^2 region in the Sierra Nevada.

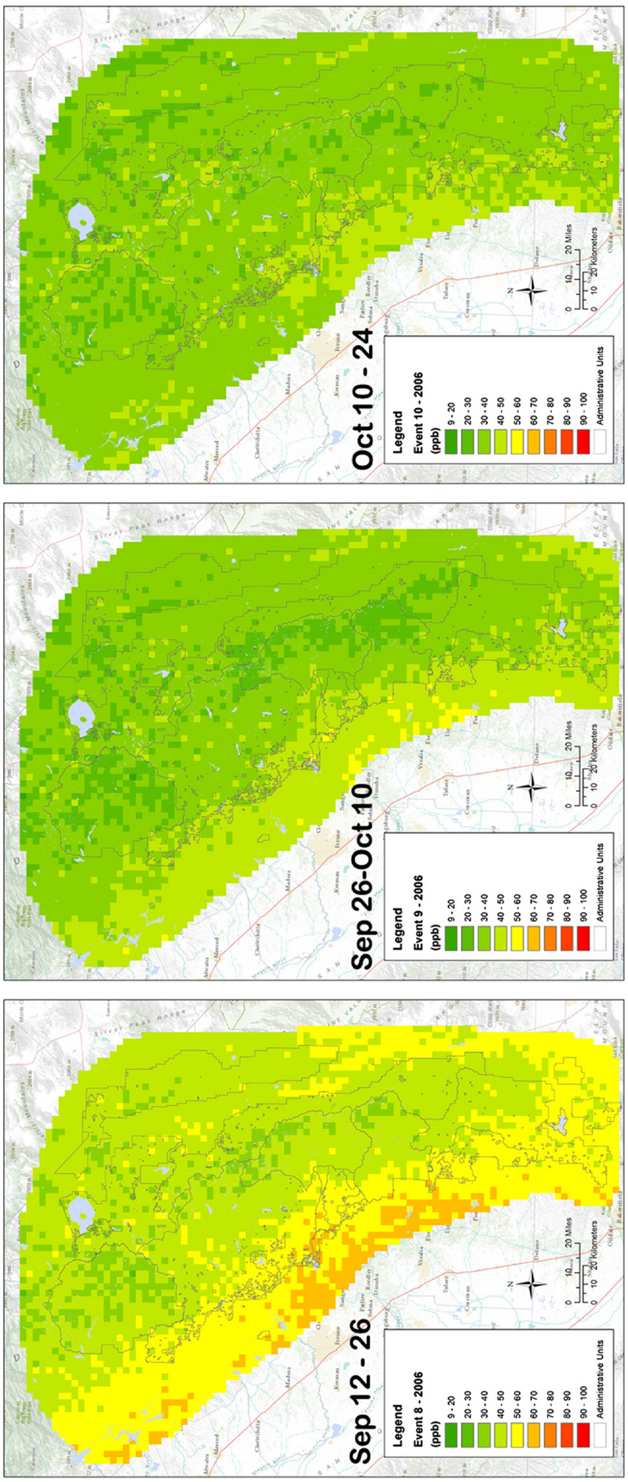

Fig. 4. (*continued*).

3.6. Analysis uncertainty

The spatial ozone concentration data were interpolated from widely spaced passive ozone monitors. Uncertainty was associated with several steps of the analysis. Uncertainty in passive ozone measurement in general in the Sierra Nevada, described as the mean absolute percent difference between ozone measured with passive samplers and continuous monitors, was investigated in an earlier study designed to assess passive monitor performance (Lee, 2003) and reported as 7.6%. When averaged over the season, it dropped to 5.8%.

Number of collectors per unit area also influenced uncertainty. Generally, the area with the greatest number of collectors per area was the western portion of the region. Here ozone concentration was highest and the concentrations were interpolated with greater certainty due to a greater number of collectors. There is significant management concern about penetration of ozone into the national parks and wilderness areas of the higher elevations and the eastern side of the Sierra. While ozone concentrations appear lower here, these areas had fewer collectors and thus lower certainty.

The goodness of fit of GWR in estimating ozone concentration surfaces was quantified through residual analysis. Mean residuals from model fit at sites on the western edge of the region were generally below 10% of the measured ozone concentration, for each of the years (Fig. 8). The remaining sites generally had mean residuals below 20%. Two sites had residuals greater than 20% in 2006. The year 2006 had greater residual magnitude than the other years, as well as greater variation in ozone concentration over time (Fig. 8). The spread of residuals in a year at each site was quantified with the standard error of the mean. Generally the westernmost sites had lowest residual standard error (Fig. 8). The spread in residuals was greatest in 2006. Thus, the GWR approach showed overall good performance in predicting ozone concentrations over the region, with residuals generally less than 20% of the observed value. The best model fit was in the westernmost part of the region, where there is generally a higher ozone signal and less complex terrain. The increasing complexity of the landscape as ozone moves eastward into the mountains likely introduces variation in ozone concentration due to microclimate, deposition to vegetation, and other factors that is not explained by the parameters of the GWR model.

The standard deviation of the mean annual ozone concentration was greatest at the westernmost extent of the region, where the episodic temporal variation in ozone concentration was most evident (Fig. 8). The standard deviation was greater over the region in 2006 than in 2007 or 2008.

3.7. Consistency with past analyses

A previous spatial analysis (Frączek, 2003) of a 1999 passive ozone network had good overlap in timing and some overlap in extent with the region of the current analysis. We sought to determine whether the two spatial ozone analyses showed similar results. The comparison method and results are shown in the Supplementary Data section.

4. Discussion

The method of combining passive ozone monitors, geographically weighted regression, and segmentation analysis has identified patterns in ozone concentration over time and over the landscape. From these analyses it was possible to identify sub-regions of potentially vulnerable forests in the Sierra Nevada region.

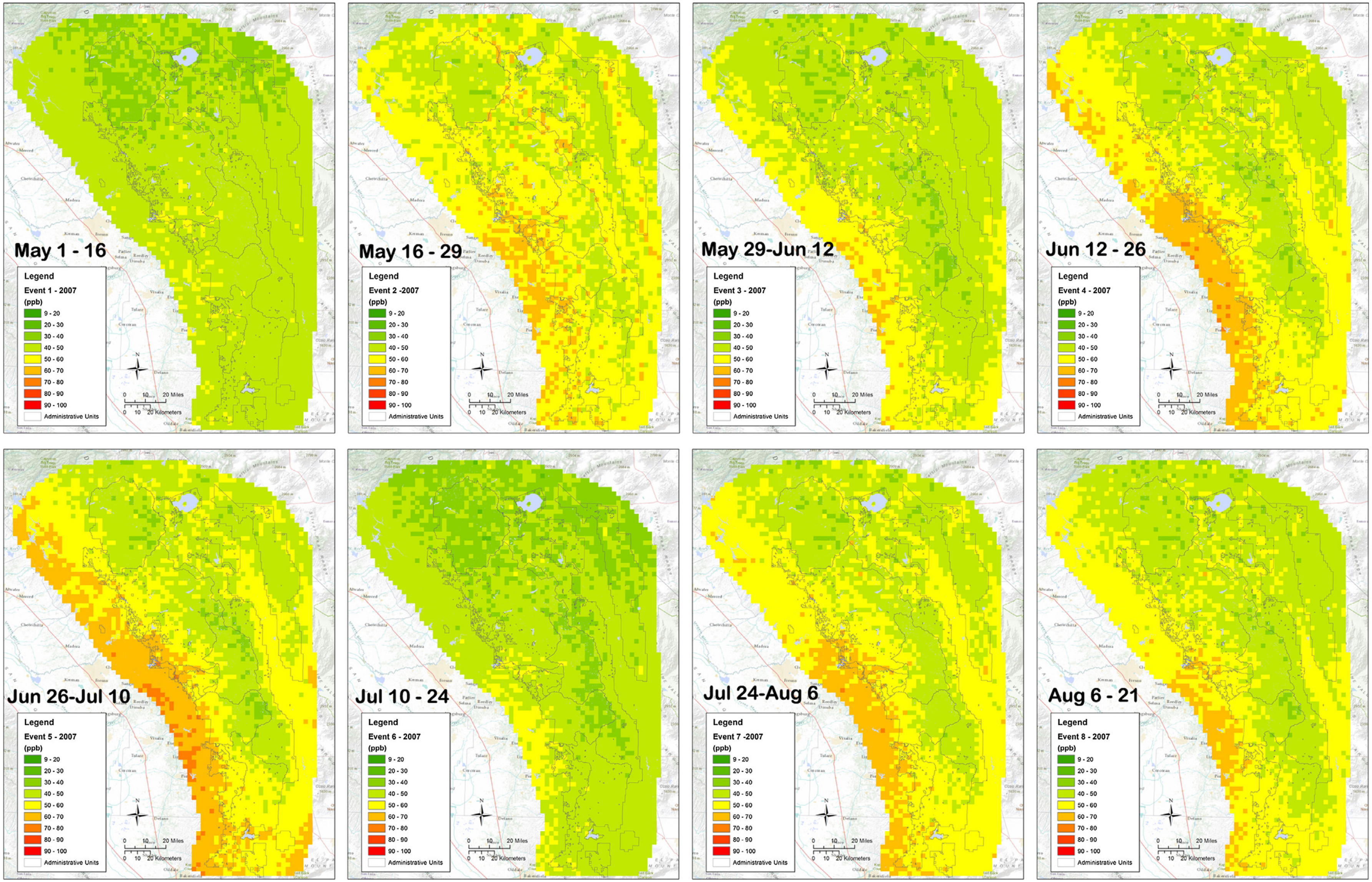

Fig. 5. Landscape patterns in ozone concentration in 2007 show temporal and spatial variation. Mean 24-h ozone concentration (ppb) for sequential two-week periods in summer-fall 2007, derived from a network of passive ozone samplers and geographically-weighted regression, are mapped across a 49,000 km^2 region in the Sierra Nevada.

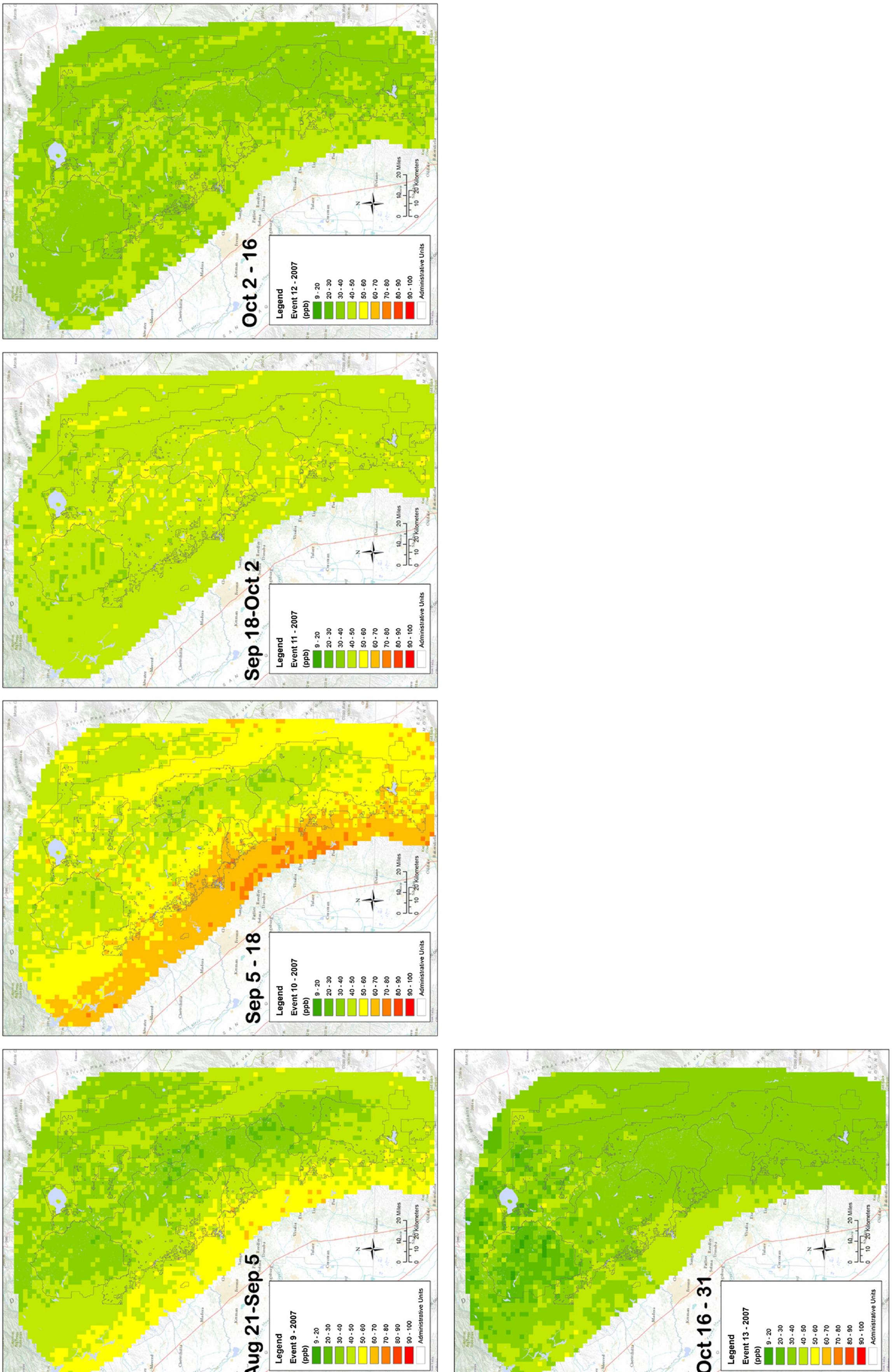

Fig. 5. (*continued*).

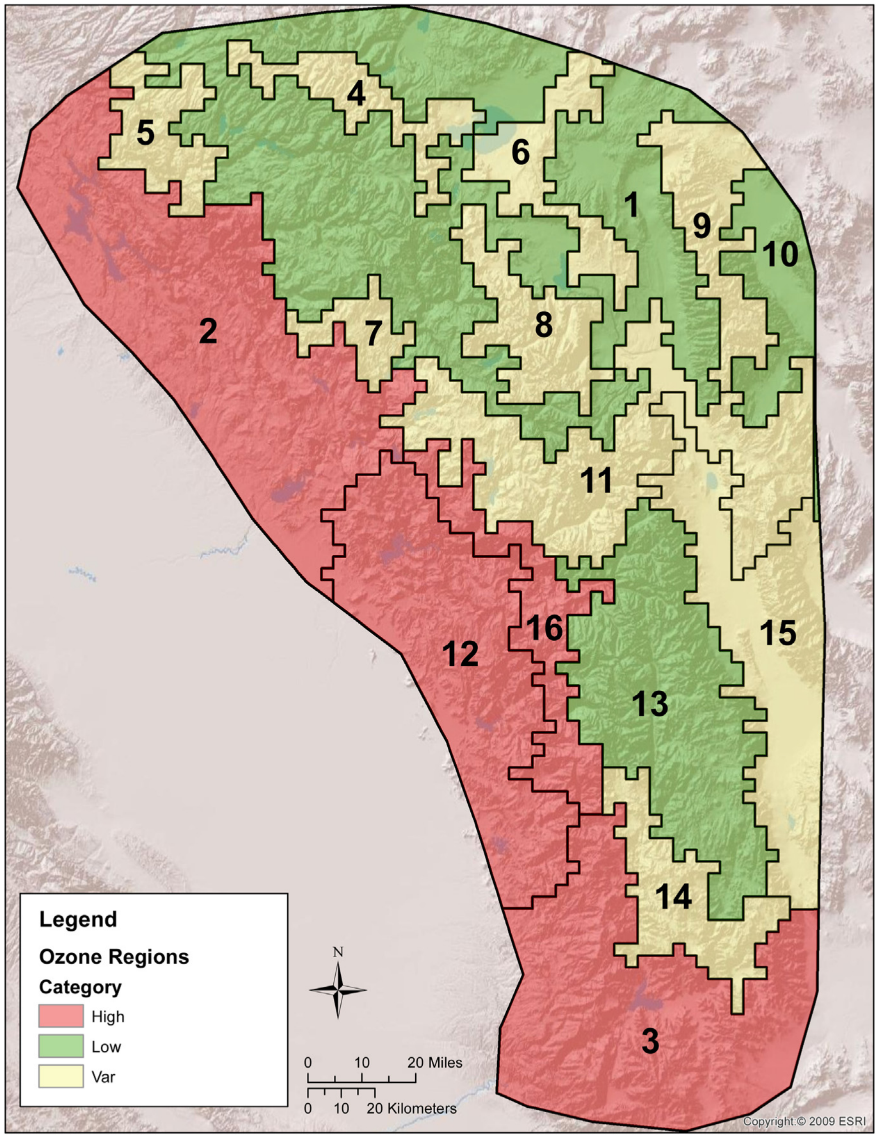

Fig. 6. Object-based image segmentation identified 16 unique sub-regions of ozone exposure that were further classified as “high”, “variable” and “low”.

Table 1
Sub-regions falling into categories of high, low or variable ozone exposure were identified using object-oriented image analysis. Each sub-region had a unique percentage of pixels in each category.

Region ID	Area (km^2)	% Low	% Variable	% High	Class
1	10,405	90%	8%	2%	Low
2	6739	0%	27%	73%	High
3	5372	0%	8%	92%	High
4	968	29%	51%	20%	Variable
5	977	9%	79%	13%	Variable
6	1170	22%	54%	24%	Variable
7	539	41%	36%	23%	Variable
8	1274	26%	59%	15%	Variable
9	1358	41%	55%	4%	Variable
10	1342	98%	2%	0%	Low
11	3957	39%	56%	4%	Variable
12	4411	0%	1%	99%	High
13	4190	85%	15%	0%	Low
14	1446	31%	55%	14%	Variable
15	3292	3%	57%	40%	Variable
16	1604	2%	29%	69%	High

4.1. Ozone exposure

Ozone concentrations in the southern Sierra Nevada showed a remarkable consistency of pattern, across time and across the landscape. Segmentation analysis revealed large areas of the region that behave similarly with respect to ozone. The western edge of the Sierra Nevada closest to the San Joaquin Valley, had the greatest ozone concentrations, with the impact of surface air pollution recirculation patterns within the San Joaquin Valley seen as a consistently higher ozone exposure area in the lower portion of its western edge. Ecosystems within this sub-region, representing roughly 10% of the entire region, were consistently exposed to the highest ozone concentrations of the entire 49,000 km^2 region.

The break delineating the edge of the high-ozone sub-regions along the western edge of the Sierra and the rest of the region to the east was at a consistent elevation of approximately 1700–2400 m (Fig. 9), analogous to a “high-tide line”. This supports the concept of a limited pollutant transport efficiency over the mountains. Other researchers have noted the break at roughly the same elevation. Bytnerowicz et al. (2002) measured pollutants along an elevational

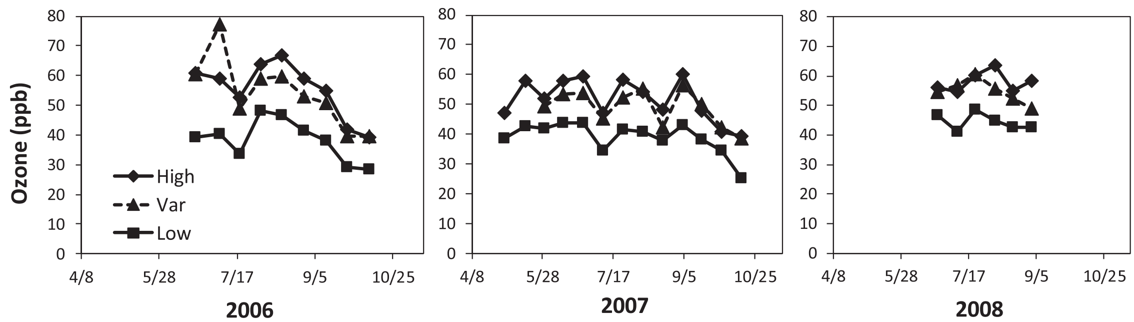

Fig. 7. Average ozone concentrations in the high and low ozone sub-region classes tracked each other consistently over time in each of three years 2006, 2007, 2008. The variable class generally tracked the other classes over time, but less consistently.

gradient in Sequoia and Kings Canyon and showed a linear drop ozone with increasing elevation between 1200 m and 2300 m. This is also consistent with Cahill et al. (1996) who showed a sharp reduction in ozone and aerosols between measurement sites in Sequoia and Kings Canyon National Parks at 1830 m and 3050 m.

The line is also likely a result of ozone loss as it moves upslope during the day and is deposited on vegetation. At night, downslope airflow brings cleaner air from aloft. Ozone does move eastward across the Sierra Nevada range, however it takes a lower elevation path. An indistinct corridor is seen in the San Joaquin River drainage area, apparent in Figs. 4 and 5. The corridor is evident in both the high, moderate and low concentration events. This transport was specifically measured by Cisneros et al. (2010) and reported in Bytnerowicz et al. (2003a).

4.2. Forest vulnerability, mortality and implications for management

The results have implications for landscape vulnerability to agents of forest mortality. Ozone-stressed pine forests have been shown to be more susceptible to pest and pathogen infestation, to drought stress, and to fire. Pines in southern California can serve as host to the western pine beetle (*Dendroctonus brevicomis* LeConte) and the mountain pine beetle (*D. ponderosae* Hopkins). Pine with measurable ozone injury show greater damage from, and less resistance to, bark beetle attack (Stark et al., 1968). In sites with high ozone and nitrogen exposure in the San Bernardino Mts., bark beetle activity and tree mortality were significantly higher than at lower exposure sites (Eatough Jones et al., 2004). Ozone-injured pine are also more likely to get infected by the pathogens annosus root disease (*Heterobasidion annosum*, James et al., 1980) and black stain root disease (Leptographium wageneri, Fenn et al., 1990).

Ozone-stressed pine forests are more susceptible to drought. Physiologically, forest exposure to ozone at moderate to high ozone exposure can lower soilwater uptake due to reduced root mass size and also increase demand for water due to loss of moisture regulation at the leaf-level (see review in Grulke et al., 2009). This enhanced susceptibility to drought would exacerbate the impact of documented increasing drought conditions in the southern Sierra brought on by decreased moisture availability due to climate change, evidenced by decreasing runoff and earlier runoff timing (Andrews, 2012; Rice and Bales, 2013).

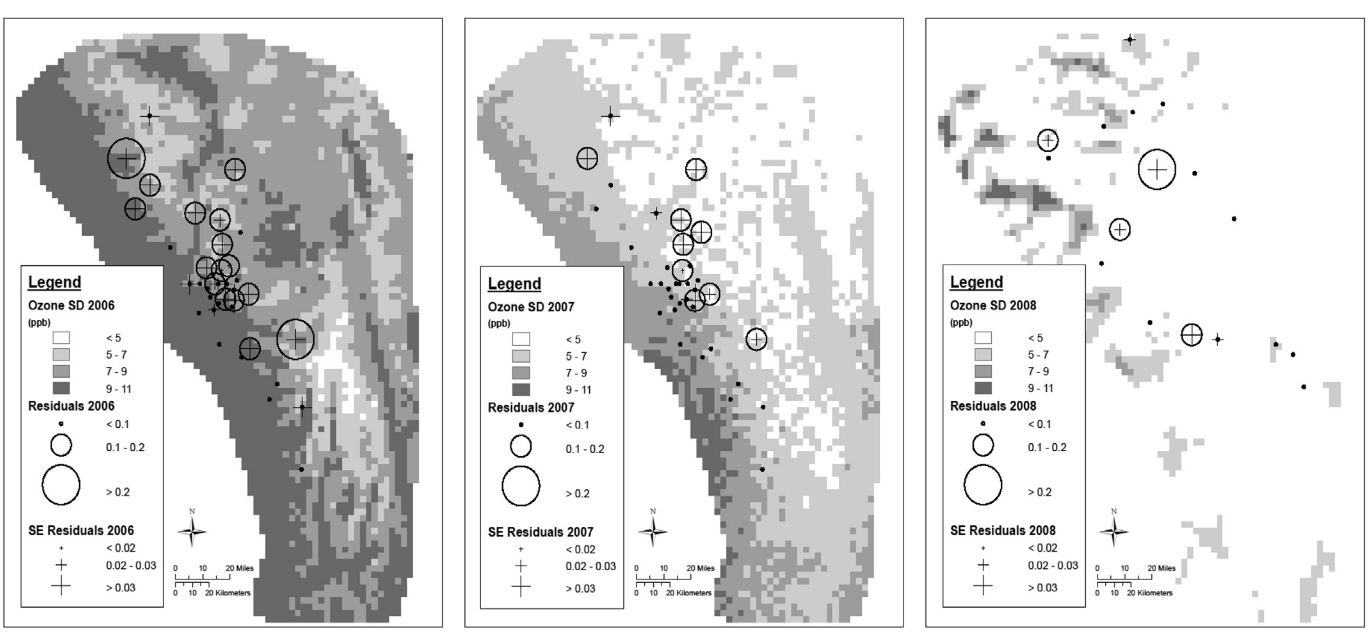

Fig. 8. Residuals (observed − predicted ozone concentration, ppb) were normalized to observed ozone concentration at each site and time. Annual mean and standard error of normalized residuals at each measurement site is plotted on a surface of standard deviation of mean modeled ozone over all two week measurement periods per cell each year.

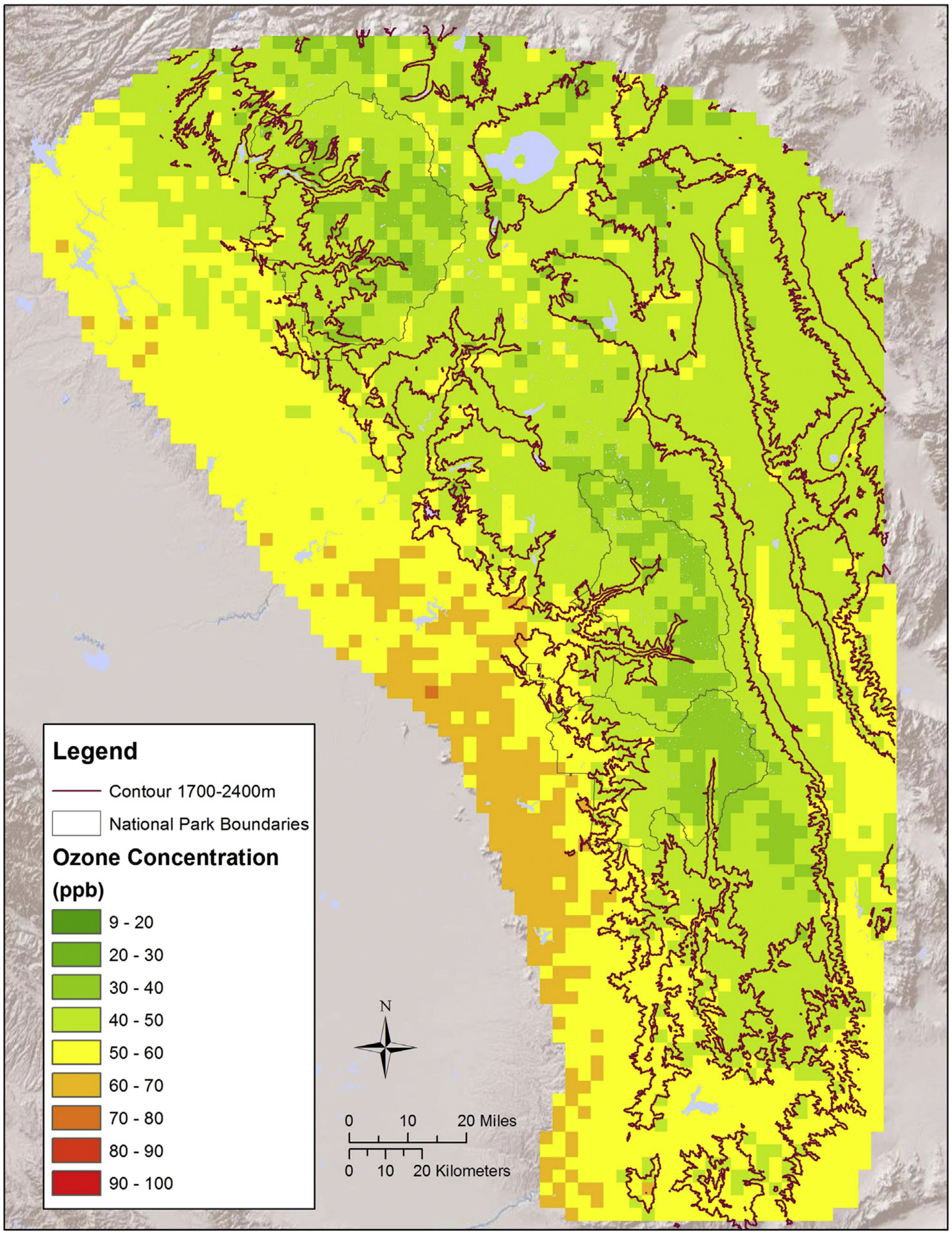

Fig. 9. The 1700–2400 m elevation band was a marked break between high and low ozone concentrations along an elevational gradient. This delineation is analogous to a "high-tide line".

Forests exposed to ozone are more susceptible to fire, both indirectly and directly. The ozone-induced forest susceptibility to bark beetles, pathogens and drought can exacerbate the risk of fire. But ozone stress in trees can directly increase fire vulnerability as well, through greater foliar loss, increased litter accumulation, and decreased litter decomposition (Grulke et al., 2009).

The pine-forested landscape along the western front of the Sierra Nevada is highly vulnerable to stress and at risk of mortality. Sub-regions 2, 12, 16, and 3 are the areas with highest ozone exposure. The western slopes of the Sierra Nevada are also experiencing increasingly longer dry seasons on average resulting in less soil moisture availability, due to earlier-season snowmelt of the mid-elevation Sierra (Andrews, 2012; Rice and Bales, 2013). Independent of these factors, the chance of fire in these regions is high, particularly in sub-regions 12, 16 and parts of 3. The interval since the last fire in these areas is 5–17 times greater than it was under historical conditions (Thorne et al., 2013), putting this area at "extreme" fire risk. With the added stress of drought and ozone, the forested regions of this area are possibly the most vulnerable to mortality in the southern Sierra Nevada.

5. Conclusions

Characterizing the spatial distribution of ozone concentration through the combined use of passive samplers and GWR quantified patterns of ozone exposure across the landscape. Some of these patterns corroborated insights inferred from other studies. Identifying zones of ozone exposure can aid in prioritizing management. Regions in the southern Sierra Nevada above 2400 m are relatively pristine. Ecosystems in high ozone concentration regions in the south and southwestern Sierra Nevada, particularly sensitive pine forests, are more vulnerable to mortality. Spatial maps of direct foliar injury on sensitive pines would provide further evidence of areas of greater and lesser forest vulnerability.

Acknowledgments

This research was funded by the National Park Service Natural Resources Condition Assessment program, particularly Sequoia and Kings Canyon National Parks, and the U.S.D.A. Forest Service Pacific Southwest Research Station. The authors thank Dr. Haiganoush Preisler for important conceptual contributions during the project. The comments of two anonymous reviewers greatly improved the manuscript.

Appendix A. Supplementary data

Supplementary data related to this article can be found at http://dx.doi.org/10.1016/j.envpol.2013.07.028.

References

Andrews, E.D., 2012. Hydrology of the Sierra Nevada Network National Parks: Status and Trends. Natural Resource Report NPS/SIEN/NRR—2012/500. National Park Service, Fort Collins, Colorado.

Arbaugh, M.J., Miller, P.R., Carroll, J.J., Takemoto, B.L., Proctor, T., 1998. Relationships of ozone exposure to pine injury in the Sierra Nevada and San Bernardino Mountains of California, USA. Environmental Pollution 101, 291–301.

Baatz, M., Schape, A., 2000. Multiresolution Segmentation, an optimization approach for high quality multi-scale image segmentation. Journal of Photogrammetry and Remote Sensing 58, 12–23.

Beaver, S., Tanrikulu, S., Palazoglu, A., Singh, A., Soong, S., Jia, Y., Tran, C., Ainsle, B., Steyn, D., 2010. Pattern-based evaluation of coupled meteorological and air quality models. Journal of Applied Meteorology and Climatology 49, 2077–2091.

Bytnerowicz, A., Tausz, M., Alonso, R., Jones, D., Johnson, R., Grulke, N., 2002. Summer-time distribution of air pollutants in Sequoia National Park, California. Environmental Pollution 118, 187–203.

Bytnerowicz, A., Padgett, P.E., Arbaugh, M.J., 2003a. Methodological needs and perspectives for monitoring ambient air pollution and regional haze, tools for understanding forest responses. pp. 263–283. In: Bytnerowicz, A., Arbaugh, M., Alonso, R. (Eds.), Ozone Air Pollution in the Sierra Nevada, Distribution and Effects on Forests, Developments in Environmental Science, vol. 2. Elsevier, Amsterdam, p. 402.

Bytnerowicz, A., Arbaugh, M.J., Alonso, R., 2003b. Ozone Air Pollution in the Sierra Nevada, Distribution and Effects on Forests. In: Developments in Environmental Science, vol. 2. Elsevier, Amsterdam, p. 402.

Bytnerowicz, A., Burley, J.D., Cisneros, R., Preisler, H.K., Schilling, S., Schweizer, D., Ray, J., Dulen, D., Beck, C., Auble, B., 2013. Surface ozone at the Devils Postpile National Monument receptor site during low and high wildland fire years. Atmospheric Environment 65, 129–141.

Cahill, T.A., Carroll, J., Campbell, D., Gill, T., 1996. Air quality. In: Status of the Sierra Nevada. Sierra Nevada Ecosystem Project. Final Report to Congress. Assessments and Scientific Basis for Management Options, vol. II. University of California, Davis, pp. 1227–1261. Wildland Resources Center Report No. 37.

California Air Resources Board (CARB), 2010. The California Almanac of Emissions and Air Quality, 2009 ed. http://www.arb.ca.gov/aqd/almanac/almanac09/almanac09.htm (accessed January 2011).

California Air Resources Board (CARB), 2013. Air Quality Data Statistics. http://www.arb.ca.gov/adam/index.html (accessed January 2013).

Carroll, J.J., Dixon, A.J., 2002. Regional scale transport over complex terrain: a case study, tracing the Sacramento plume in the Sierra Nevada of California. Atmospheric Environment 36, 3745–3758.

Cisneros, R., Bytnerowicz, A., Schweizer, D., Zhong, S., Traina, S., Bennett, D.H., 2010. Ozone, nitric acid, and ammonia air pollution is unhealthy for people and ecosystems in southern Sierra Nevada, California. Environmental Pollution 158, 3261–3271.

De Marco, A., Screpanti, A., Paoletti, E., 2010. Geostatistics as a validation tool for setting ozone standards for durum wheat. Environmental Pollution 158, 536–542.

Denby, B., Cassiani, M., de Smet, P., de Leeuw, F., Horálek, J., 2011. Sub-grid variability and its impact on European wide air quality exposure Assessment. Atmospheric Environment 45, 4220–4229.

Duriscoe, D.M., 1990. Cruise Survey of Oxidant Air Pollution Injury to *Pinus ponderosa* and *Pinus jefferyi* in Saguaro National Monument, Yosemite National Park, and Sequoia and Kings Canyon National Parks. NPS/ADQ-90/003. Air Division, Quality Division, U.S. Department of the Interior, National Park Service, Denver, CO, p. 68.

Eatough Jones, M., Paine, T.D., Fenn, M.E., Poth, M.E., 2004. Influence of ozone and nitrogen deposition on bark beetle activity under drought conditions. Forest Ecology and Management 200, 67–76.

Fenn, M.E., Dunn, P.H., Wilborn, R., 1990. Black stain root disease in ozone-stressed ponderosa pine. Plant Disease 74, 426–430.

Finke, T., Moran, S., Yool, S., Kennedy, J., 2009. Object-oriented classification to map impervious surfaces for hydrologic models. In: Papers from the Annual Meeting of the Association of American Geographers – 2009. Association of American Geographers, Las Vegas, NV.

Forthofer, J., Butler, B., 2013. Windninja. http://www.firelab.org/research-projects/physical-fire/145-windninja (accessed 12.03.13.).

Frączek, W., 2003. Use of geostatistics to estimate surface ozone patterns. pp. 215–247. In: Bytnerowicz, A., Arbaugh, M.J., Alonso, R. (Eds.), Ozone Air Pollution in the Sierra Nevada, Distribution and Effects on Forests, Developments in Environmental Science, vol. 2. Elsevier, Amsterdam, p. 402.

Grulke, N.E., Minnich, R.A., Paine, T.D., Seybold, S.J., Chavez, D.J., Fenn, M.E., Riggan, P.J., Dunn, A., 2009. Air pollution increases forest susceptibility to wildfires, a case study in the San Bernardino mountains in southern California (Chapter 17). In: Bytnerowicz, A., Arbaugh, M., Riebau, A., Andersen, C. (Eds.), Wildland Fires and Air Pollution, Developments in Environmental Science, vol. 8. Elsevier, Amsterdam, p. 686.

InciWeb, 2006. http://www.wildlandfire.com/arc/socalfires06.htm (accessed January 2013).

James, R.L., Cobb, F.W., Wilcox, W.W., Rowney, D.L., 1980. Effects of photochemical oxidant injury of ponderosa and Jeffrey pines on susceptibility of sapwood and freshly cut stumps to *Fomes annosus*. Phytopathology 70, 704–708.

Kampouraki, M., Wood, G.A., Brewer, T.R., 2008. Opportunities and limitations of object based image analysis for detecting urban impervious and vegetated surfaces using true-colour aerial photography. In: Object-based Image Analysis. Springer, Berlin, pp. 555–569.

Koutrakis, P., Kelly, B.P., 1993. Measurement of ambient ozone using a nitrite-coated filter. Analytical Chemistry 65, 209–214.

Krupa, S.V., Legge, A.H., 2000. Passive sampling of ambient gaseous air pollutants, an assessment from an ecological perspective. Environmental Pollution 107, 31–45.

Lee, H.E., 2003. Use of auxiliary data for spatial interpolation of surface ozone patterns pp 165-194. In: Bytnerowicz, A., Arbaugh, M.J., Alonso, R. (Eds.), Ozone Air Pollution in the Sierra Nevada, Distribution and Effects on Forests, Developments in Environmental Science, vol. 2. Elsevier, Amsterdam, p. 402.

Loibl, W., Winiwarter, W., Kopsca, A., Zufger, J., Baumann, R., 1994. Estimating the spatial distribution of ozone concentrations in complex terrain. Atmospheric Environment 28, 2557–2566.

Miller, P.R., Millecan, A.A., 1971. Extent of oxidant air pollution injury to some pines and other conifers in California. Plant Disease Reporter 55, 555–559.

Miller, J.E., Nelson, S.A.C., Hess, G.R., 2009. An object extraction approach for impervious surface classification with very-high-resolution imagery. The Professional Geographer 61.

Olson, C.E., 1960. Elements of photographic interpretation common to several sensors. Photogrammetric Engineering 26 (4), 651–656.

Panek, J.A., 2004. Ozone uptake, water loss and carbon exchange dynamics in annually drought-stressed *Pinus ponderosa* forests: measured trends and parameters for uptake modeling. Tree Physiology 24, 277–290.

Panek, J.A., Goldstein, A.H., 2001. Responses of stomatal conductance to drought in ponderosa pine: implications for carbon and ozone uptake. Tree Physiology 21, 337–344.

Panek, J.A., Saah, D.S., Esperanza, A., 2013. A natural resource condition assessment for Sequoia and Kings Canyon National Parks: Appendix 2 – Air Quality, 2013, National Park Service; Fort Collins, Colorado, National Park Service, Natural Resource Report. NPS/SEKI/NRR—2013/665.2.

Pfister, G.G., Wiedinmyer, C., Emmons, L.K., 2008. Impacts of the fall 2007 California wildfires on surface ozone, integrating local observations with global model simulations. Geophysical Research Letters 35. L19814, 5.

Preisler, H.K., Schilling, S.L., 2003. Use of nonparametric local regression to estimate surface ozone patterns. pp. 195–214. In: Bytnerowicz, A., Arbaugh, M.J., Alonso, R. (Eds.), Ozone Air Pollution in the Sierra Nevada, Distribution and Effects on Forests, Developments in Environmental Science, vol. 2. Elsevier, Amsterdam, p. 402.

Rice, R., Bales, R.C., 2013. A Natural Resource Condition Assessment for Sequoia and Kings Canyon National Parks: Appendix 7-Rain, Snow, Temperature. National Park Service, Fort Collins, Colorado. National Park Service. 2013. Natural Resource Report NPS/SEKI/NRR—2013/665.7.

Singh, V., Carnevale, C., Finzi, G., Pisoni, E., Volta, M., 2011. A cokriging based approach to reconstruct air pollution maps, processing measurement station concentrations and deterministic model simulations. Environmental Modelling & Software 26, 778–786.

Stark, R.W., Miller, P.R., Cobb, F.W., Jr., 1968. Photochemical oxidant injury and bark beetle (Coleoptera: Scolytidae) infestation of ponderosa pine. I. Incidence of bark beetle infestation in injured trees. Hilgardia 39, 121–152.

Thomas, N., Hendrix, C., Congalton, R.G., 2003. A comparison of urban mapping methods using high-resolution digital imagery. Photogrammetric Engineering and Remote Sensing 69 (9), 963–972.

Thorne, J., Monahan, W.B., Holguin, A., Schwartz, M., 2013. A Natural Resource Condition Assessment for Sequoia and Kings Canyon National Parks: Appendix 1-Landscape Context. National Park Service, Fort Collins, Colorado. National Park Service. 2013. Natural Resource Report NPS/SEKI/NRR—2013/665.1.

United States Environmental Protection Agency (USEPA), 2011. EPA Home/Region 9/Air/Actions/California/San Joaquin Valley Ozone. http://www.epa.gov/region9/air/sjvalley/ (accessed January 2011).

Van Mantgem, P.J., Stephenson, N.L., Mutch, L.S., Johnson, J., Esperanza, A.M., Parsons, D.J., 2003. Growth rate predicts mortality of *Abies concolor* in both burned and unburned stands. Canadian Journal of Forest Research 33, 1029–1038.

Van Ooy, D.J., Carroll, J.J., 1995. The spatial variation of ozone climatology on the western slope of the Sierra Nevada. Atmospheric Environment 29, 1319–1330.

Weaver, C.P., Liang, X.-Z., Zhu, J., Adams, P.J., Amar, P., Avise, J., Caughey, M., Chen, J., Cohen, R.C., Cooter, E., Dawson, J.P., Gilliam, R., Gill iland, A., Goldstein, A.H., Grambsch, A., Grano, D., Guenther, A., Gustafson, W.I., Harley, R.A., He, S., Hemming, B., Hogrefe, C., Huang, H.-C., Hunt, S.W., Jacob, D.J., Kinney, P.L., Kunkel, K., Lamarque, J.-F., Lamb, B., Larkin, N.K., Leung, L.R., Liao, K.-J., Lin, J.-T., Lynn, B.H., Manomai phi boon, K., Mass, C., McKenzie, D., Mickley, L.J., O'Neill, S.M., Nolte, C., Pandis, S.N., Racherla, P.N., Rosenzweig, C., Russell, A.G., Salathé, E., Steiner, A.L., Tagaris, E., Tao, Z., Tonse, S., Wiedinmyer, C., Williams, A., Winner, D.A., Woo, J.-H., Wu, S., Wuebbles, D.J., 2009. A preliminary synthesis of modeled climate change impacts on U.S. regional ozone concentrations. Bulletin of the American Meteorological Society 90, 1843–1863.

Wong, D.W., Yuan, L., Perlin, S.A., 2004. Comparison of spatial interpolation methods for the estimation of air quality data. Journal of Exposure Analysis and Environmental Epidemiology 14, 404–415.